Four-Level Optical Line Shape of a Single Molecule Coupled to a Single Tunneling Two-Level System †

ARTICLE *in* THE JOURNAL OF PHYSICAL CHEMISTRY B · OCTOBER 2006

Impact Factor: 3.3 · DOI: 10.1021/jp0574908 · Source: PubMed

2 AUTHORS, INCLUDING:

Michel Orrit
Leiden University
207 PUBLICATIONS **8,978** CITATIONS

Four-Level Optical Line Shape of a Single Molecule Coupled to a Single Tunneling Two-Level System†

Clemens Hofmann and Michel Orrit*

Molecular Nano-Optics and Spins (MoNOS), Huygens Laboratory, Postbus 9504, University of Leiden, 2333 CA Leiden, The Netherlands

Received: December 23, 2005; In Final Form: June 14, 2006

We propose a density-matrix theory for the four-level system consisting of a single optical two-level system (OTLS) coupled to a single two-level system tunneling along a vibrational coordinate (VTLS). Phonons induce jumping rates of the VTLS, but coherent tunneling has to be considered explicitly as well, because the Born−Oppenheimer potential of the tunnel variable may change upon optical excitation. The OTLS is subject to spontaneous emission and driven by a laser wave with arbitrary strength. Numerical simulations for various coupling cases reproduce limiting behaviors previously discussed separately in the literature, such as motional narrowing, cross transitions, optical saturation and pumping, and nonlinear effects. Our model also perfectly fits recent measurements of the spectra of a single molecule coupled to a single tunneling system in a disordered crystal.

1. Introduction

The interaction of an atom or molecule with an intense laser field can be described as a magnetic resonance experiment on an effective two-level system or spin-$^1/_2$, as pointed out by Feynman et al.[1] In this model, the interactions of the optical two-level system (OTLS) with baths lead to two relaxation rates, one for the population of the excited state and one for the coherence between ground state and excited state. Whereas the bath of empty photon modes is responsible for excited state relaxation by spontaneous emission, the bath of phonons (in condensed matter) or of colliding particles (in gas phase) leads to the fast fluctuations of the optical transition frequency responsible for a loss of memory of the phase, a process called pure dephasing or decoherence. The latter dephasing process can only be rigorously described in a density matrix formalism. The resulting optical Bloch equations successfully describe many experimental systems, from atoms[2] to single molecules in condensed matter,[3] to an amazing degree of accuracy and intrication. Yet, the use of Bloch rate parameters supposes a crucial condition: The typical fluctuation times of the baths must be much shorter than any other characteristic time of the system. This inequality is often violated in condensed matter, for example, in disordered crystals or in glasses, where characteristic times cover a broad range extending from picoseconds to days and beyond. Upon a slow change of the environment, the frequency of the OTLS slowly varies in time, a phenomenon referred to as spectral diffusion, because the OTLS's line then slowly diffuses in the one-dimensional frequency space. The simplest model of spectral diffusion is obtained by coupling the OTLS to a single low-frequency two-level system. This latter spin-$^1/_2$ corresponds to motion along a vibrational coordinate. We shall therefore call it the "vibrational" two-level system (VTLS) in this article. The OTLS−VTLS coupled system has much in common with an electron spin-$^1/_2$ coupled to a nuclear spin-$^1/_2$, but important differences characterize the optical case and warrant a special treatment. Two of the specific features are spontaneous emission, which introduces an asymmetry between ground and excited states of the OTLS, and the change of potential profile of the VTLS upon excitation of the OTLS, which can be considerable.

Several previous theoretical papers have dealt with various versions of this four-level model. The semiclassical model of Kubo[4] and Anderson[5] postulates sudden jumps of the VTLS, which modulate the optical frequency of the OTLS. If the dwell time in one of the states of the VTLS is longer than the inverse of the frequency jump, the corresponding state will give rise to an isolated sharp line in the OTLS's absorption spectrum. On the other hand, if the dwell times in either VTLS state are shorter than the inverse of the frequency jump, only a single line is observed at the average frequency, and its broadening decreases for increasing jump rate. This limit, called motional narrowing, is common in magnetic resonance at room temperature but unusual in optical spectroscopy. Later versions of the theory[6−10] have addressed the fully quantum-mechanical version of the four-level system, based on Mori's or Redfield's theory for the density matrix.[11−15] This theory introduces additional relaxation rates for populations and coherences of the 4×4 density matrix which leads to a coupled system of 16 differential equations. These treatments were restricted to low laser power. Few attempts have been made at writing and solving the master equation for the general case of arbitrary laser field strength, on one hand because of the complexity of the problem but also, on the other hand, for lack of experimental observations to determine the many parameters required by the model. Plakhotnik[16] has treated the quantum-mechanical four-level system in an intense laser field, but with the same VTLS eigenstates in the ground and excited OTLS states, which considerably simplifies the problem by eliminating two of the four possible transitions.

† Part of the special issue "Robert J. Silbey Festschrift".

* To whom correspondence may be addressed. E-mail: orrit@molphys.leidenuniv.nl).

10.1021/jp0574908 CCC: $33.50
Published on Web 08/11/2006

Much attention for the theory of four-level systems arose in the field of low-temperature optical spectroscopy of molecules, ions, and more recently of small semiconductor nanoparticles. In the latter case, a description of the nanoparticle as an OTLS is only possible if the particle is small enough to consider its lowest optical transition as isolated. In condensed matter, the OTLS is usually coupled to elementary excitations of the surrounding host material. For glasses, polymers, or even for disordered crystals at low temperatures, the relevant excitations are usually modeled as two-level systems (VTLSs).[17,18] The rationale for this simplification of the complex potential landscape of a glass is that, among the many nearly degenerate wells of the potential, tunneling occurs preferentially between pairs of wells located nearby, in comparatively small areas of the glass. The relaxation may therefore be modeled as an ensemble of spin-$^1/_2$ systems, as borne out by a wide variety of experiments on ensembles[19] and, more recently, by single-molecule spectroscopy.[20] For ensemble experiments in a disordered system, one in principle expects wide distributions of couplings and jumping times, so that all cases of couplings, slow as well as fast modulations, will contribute to the average. Theories for ensemble experiments have therefore always included some averaging over OTLSs and/or over the distributions of VTLSs around them. The observation of the line shapes of individual molecules with high-resolution spectroscopy has introduced a novel approach to the classic problem of the four-level system. Indeed, single-molecule observations make detailed investigation of the OTLS line shape possible without inhomogeneous broadening and without averages over ill-known distributions. Moreover, in many crystals or disordered matrixes, the concentration of VTLSs is low enough that a single optical center (often an organic molecule in actual experiments) is strongly coupled to mostly one single VTLS. Therefore, single-molecule observations provide ideal instances of OTLS−VTLS coupled systems, where all relevant parameters can be determined experimentally on a few spectra and more complex spectra can be compared to calculations. A very similar approach was recently demonstrated by Hettich et al.[21] and by Hofmann et al.[22] for the problem of two or more OTLSs coupled by dipole−dipole excitonic interactions.

The aim of present paper is to introduce a general formalism for an arbitrary case of OTLS−VTLS coupling, including coherent tunneling of the VTLS in the ground and excited states of the OTLS, jumps between the tunnel states, and arbitrary laser intensity. Those are necessary improvements of the conventional theory, in which the VTLS states are usually written in the eigenbasis of tunnel states. As these states may radically change upon excitation (in the Born−Oppenheimer approximation, the potential curves of the VTLS in principle differ in ground and excited OTLS states), the treatment of optical transitions requires a common basis for the vibrational variable, for example, the localized basis of the tunnel system chosen here. For simplicity sake, we consider a VTLS tunneling between the same localized two wells, only with different tunneling asymmetries and tunneling matrix elements in the ground and excited OTLS states. The VTLS eigenstates therefore differ in the two OTLS states. Finally, by coupling the VTLS to a bath of acoustic phonons, we obtain jump rates between the tunnel eigenstates. To reduce the number of adjustable parameters, we further neglect optical[23] and VTLS[24] dephasing induced by phonons. Limiting cases of this general problem were discussed earlier in the literature:

In the absence of the VTLS, the OTLS obeys optical Bloch equations.[14,25] The optical resonance is Lorentzian, with a width given by the dephasing rate $1/T_2$, itself determined by the excited state's inverse lifetime $1/T_1$. At high laser intensity, the line is broadened by optical saturation.

In the simplest picture, classical VTLS jumps can be seen as modulating the quantum OTLS coherence frequency in a semiclassical way. Very fast jumps of the VTLS cause a new channel for the loss of the phase of the OTLS, pure dephasing, due to a random walk of the phase. When the jump rate of the VTLS decreases to become comparable to the frequency change of the OTLS, the line shape broadens and splits into two Lorentzian components.[1,4,5,26] For slow modulation, these components correspond to the VTLS sitting in either well, and the OTLS absorbs at either of the two corresponding frequencies. In this spectral diffusion limit, the line of a single OTLS can be followed as a function of time as it jumps back and forth between its two positions.

The quantum-mechanical version of the sudden jump model requires more parameters than the above semiclassical version but basically yields the same qualitative transition between spectral diffusion and dephasing. Its treatment using Redfield equations has been given in several papers[7,9,13] and forms the basis of our theory of section 2.

Tunnel matrix elements between VTLS states can in principle be included by renormalizing VTLS states in each OTLS state. However, the tunnel eigenstates generally differ in the ground and excited state of the OTLS, which leads to four allowed optical transitions, instead of only two in the former model. Each of these transitions presents a different saturation intensity, which depends on the tunnel element and on the dephasing and relaxation rates. The line shape may therefore not only broaden but qualitatively change upon a change of excitation power. In section 3, we shall see examples of this behavior of the four-level system, which, to our knowledge, has not been discussed before.

Glasses are not the only materials displaying two-level excitations at low temperature. Tunnel systems can also be expected in weakly conducting systems where charge carriers can hop from site to site. This is actually the main motivation for the study presented here.[27] Although the coupled OTLS−VTLS is nothing else than a (deceptively) simple four-level system, as we shall show, it displays an astonishing complexity and richness of behavior. In section 2 of this paper, we present a theory based on Liouville equations for the density matrix of the four-level system. In addition to a Hamiltonian evolution under laser excitation and tunneling, we introduce the two baths of empty photon modes (causing spontaneous emission) and of lattice phonons (inducing relaxation between the tunneling levels). The 16×16 Liouville matrix is too complex for analytical solution. In section 3, we present numerically calculated line shapes where we vary such parameters as the jump rates, the asymmetry and tunneling element of the VTLS, and the laser power. In particular, we revisit a single-molecule measurement by Bauer and Kador,[28,29] for which all parameters can be determined using our theory. A final section gives the main conclusions and outlook of this work.

2. Theory

In the model we describe in the following, we consider the simplest case of the interaction between a single VTLS and a chromophore; see Figure 1. We treat the chromophore as an OTLS having a ground, $|g\rangle$, and an electronically excited, $|e\rangle$, state with an energy difference ω_{eg}. The VTLS is assumed to be made up of two states, left $|L\rangle$, and right $|R\rangle$ on either side of a barrier with an energy asymmetry Δ. A tunneling matrix

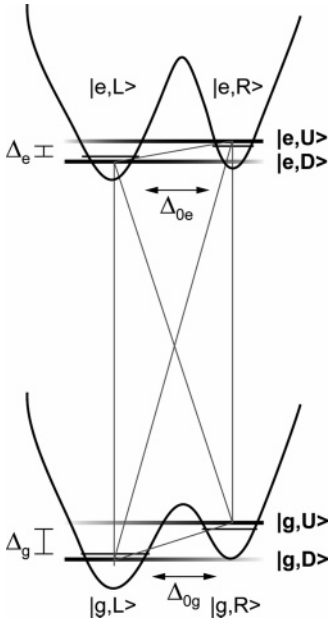

Figure 1. Four-level system consisting of an optical two-level system with a ground $|g\rangle$ and an excited $|e\rangle$ state and a vibronic two-level system with a left $|L\rangle$ and a right $|R\rangle$ state. The VTLS is represented by a two-well potential in each of the states of the OTLS and the localized states are depicted by a thin black line in each of the wells. The VTLS has an energy asymmetry Δ_g and Δ_e and a tunneling constant Δ_{0g} and Δ_{0e} in the ground and excited state of the OTLS, respectively. This coupling leads to the delocalized states $|U\rangle$ and $|D\rangle$ which are indicated by the thick shaded lines. The thin gray lines indicate possible transitions between the four states; four of them occur at optical frequencies.

element Δ_0 couples the left and right wells. The VTLS parameters can differ for ground and excited states of the OTLS. In the localized basis, the Hamilton matrix of the VTLS is

$$H_{\mathrm{VTLS}\ i} = \begin{pmatrix} 0 & -\Delta_{0i} \\ -\Delta_{0i} & \Delta_i \end{pmatrix} \tag{1}$$

where the index i refers to the state of the chromophore (i.e., g or e). In the delocalized basis, the up, $|U\rangle$ and down, $|D\rangle$ eigenstates of H_{VTLS} are

$$|U\rangle = -\sin\theta/2|L\rangle + \cos\theta/2|R\rangle \tag{2}$$

$$|D\rangle = \cos\theta/2|L\rangle + \sin\theta/2|R\rangle \tag{3}$$

where $\cos\theta = \Delta/(\Delta^2 + 4\Delta_0^2)^{1/2}$ and $\theta \in [0,\pi]$. (A note should be made on the tunneling matrix element. Commonly, the matrix element is dominated by the kinetic energy in the barrier region and its sign is determined by the choice of relative signs for the localized wavefunctions.[8,30] Either way, $|D\rangle$ is the symmetric and $|U\rangle$ the antisymmetric state in the delocalized basis. However, if the tunneling matrix element is dominated by the potential energy, for a low barrier height, the $|D\rangle$ state will be antisymmetric (see eq 1.5 in ref 19).)

The corresponding eigenvalues E_U and E_D of the energetically upper $|U\rangle$ and lower $|D\rangle$ states are

$$E_{\mathrm{U/D}} = \frac{1}{2}\Delta \pm \sqrt{\Delta_0{}^2 + \frac{1}{4}\Delta^2} \tag{4}$$

Applying a laser field $\vec{E}$ will couple the ground and excited states of the OTLS introducing matrix elements in the form of $\vec{\mu} = \langle g, L|\vec{d}|e, L\rangle$, where $\vec{d}$ is the dipole operator with $\Omega = |\vec{\mu}\vec{E}|/\hbar$ the Rabi frequency and $\vec{\mu}$ the transition-dipole moment. In line with the Herzberg−Teller approximation, we assume that the laser only acts on the OTLS dipole operator. We will furthermore consider only near-resonance excitation and invoke the rotating wave approximation.

In the next step we introduce a perturbation of the four-level system (FLS) by the baths of photons and phonons. The empty photon modes will induce spontaneous emission from the excited to the ground state of the OTLS, whereas the phonons will induce transitions between the upper and lower states of the VTLS. The total Hamiltonian of this system is given by

$$H = H_{\mathrm{FLS}} + H_{\mathrm{R}} + V \tag{5}$$

where H_{FLS} represents the FLS, H_{R} the baths of photons and phonons, and V the interaction between the baths and the FLS.

However, as the baths contain an infinite number of degrees of freedom, the joint system and bath phase space is too complex and cannot be treated explicitly. To overcome this problem, we assume that the correlation time of the bath is much shorter than the correlation time of the FLS. Therefore we introduce two projection operators P and Q which partition the joint phase space into two parts, that of the FLS and that of the baths, respectively. We can then describe the FLS by the reduced system density operator $\rho = P\rho_T = \mathrm{Tr}_R(\rho_T)$ in the phase space of the FLS instead of the total density operator ρ_T of the FLS and the baths. The reduced density matrix will comprise 16 matrix elements $\rho^*_{mn} = \rho_{nm}$. The four diagonal elements represent the populations (g_L, g_R, e_L, e_R) and the upper off-diagonal elements six coherences (ρ_{gLeL}, ρ_{gReR}, ρ_{gLeR}, ρ_{gReL}, ρ_{gLgR}, ρ_{eLeR}) where ρ_{nm} represents the coherence between states n and m. The coherences carry a real and an imaginary part and therefore represent 12 independent real variables.

In second-order perturbation theory we can then describe the evolution of the reduced density operator by the Liouville equation

$$\dot{\rho} = \frac{1}{i\hbar} P\mathscr{L}_{\mathrm{eff}} P(\rho) \tag{6}$$

where

$$P\mathscr{L}_{\mathrm{eff}} P = P(\mathscr{L}_{\mathrm{FLS}} + \mathscr{L}_{\mathrm{R}})P + P\mathscr{R}P \tag{7}$$

is the effective Liouville operator, with the relaxation super operator

$$P\mathscr{R}P = P\Lambda Q \frac{1}{\zeta - \mathscr{L}_{\mathrm{FLS}} - \mathscr{L}_{\mathrm{R}}} Q\Lambda P \tag{8}$$

$\mathscr{R}$ gives rise to matrix elements of the form $\langle\rho_{ij}|\mathscr{R}|\rho_{kl}\rangle = \mathscr{R}_{ijkl}$ with $\zeta = E_j - E_i$ and $\Lambda\,|\rho\rangle = |[V,\rho]\rangle$. $\mathscr{R}_{ijkl}$ thus describes the bath-induced contribution to the rate of change of the density matrix element ρ_{ij} proportional to the density matrix element ρ_{kl}.

The empty photon bath causes spontaneous emission with a rate Γ from the excited to the ground OTLS state, whereas it does not affect the state of the VTLS. From the relaxation superoperator we can determine the rates of the population and coherence decays in the OTLS as well as the rate of coherence transfer from the VTLS in the excited OTLS-state to the VTLS in the ground OTLS state. The coherence rates contain in principle real and imaginary parts. The real parts cause shifts of the adjustable transition frequencies. As is customary, we assume that they are included in the observed frequencies and shall neglect them. One must remember, however, that these shifts depend on ζ and on all other parameters of the calculation.

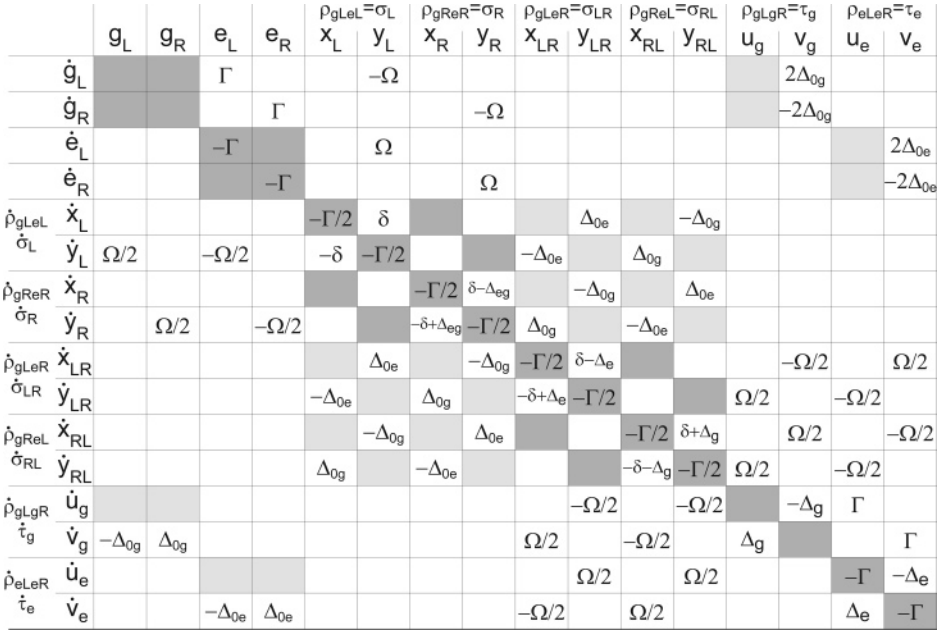

Figure 2. Master equation of the four-level system. It displays the equations of motion of the elements of the reduced density matrix ρ. The populations g_L, g_R, e_L, e_R are real numbers whereas the coherences ρ_{gLeL}, ρ_{gReR}, ρ_{gLeR}, ρ_{gReL}, ρ_{gLgR}, ρ_{eLeR} are complex numbers with a real (x or u) and an imaginary (y or v) part. Γ is the spontaneous emission rate, Ω the Rabi frequency, and δ the laser detuning. The other variables were already defined in Figure 1, with $\Delta_{eg} = \Delta_e - \Delta_g$. The gray shaded matrix elements indicate the contributions of the phonon rates which can no longer be written in a compact analytical form after the coordinate transformation back to the localized basis of the VTLS. The dark gray elements represent the position of the nonzero elements in the initial delocalized basis (the density matrix being written in the tunnel eigenbasis with L → D and R → U). The lighter gray elements are zero in the delocalized basis and appear upon coordinate transformation to the localized basis.

Assuming the shift to be included in a constant transition frequency amounts to neglecting this dependency and may lead to inconsistencies and inaccuracies for very large values of the bath-induced rates (see section 3).

The phonon bath causes population transfer, coherence decay, and coherence transfer in the VTLS. In contrast to the photon bath, which is empty, the phonon bath leads not only to emission but also to the absorption of phonons by the VTLS. To limit the number of parameters in our model, we will neglect pure dephasing induced by phonons and associated coherence transfer. We only consider population relaxation rates, together with the associated rates of coherence loss and transfer. In contrast to the $\mathscr{R}$ for the photons, which is diagonal in the localized state of the VTLS, $\mathscr{R}$ for the phonons is diagonal in the delocalized (i.e., the $|U\rangle$, $|D\rangle$) basis. We will therefore introduce a phonon-induced rate k of downhill relaxation of the VTLS (i.e., $|U\rangle \rightarrow |D\rangle$ and a rate l for uphill relaxation. The ratio of these rates is given by the Boltzmann law $k/l = \exp((E_U - E_D)/k_BT)$. Although these relaxation rates depend on the tunnel splitting and states, and therefore in principle differ in the two OTLS states, we chose the same values in both states for our simulations of section 3, to limit the number of adjustable parameters.

We have first calculated $\mathscr{L}_{FLS}$ of the OTLS and VTLS by using the Hamilton matrix of the VTLS from eq 1 and the coupling of the excited and ground states of the OTLS by the Rabi frequency. Second, we have calculated the matrix elements of the relaxation superoperator induced by the photon and the phonon baths. Having thus solved the Liouville equation from eq 6, we finally arrive at the equations of motion for the reduced density operator in the phase space of our FLS which are shown in Figure 2.

The effective Liouville operator, as depicted in Figure 2, is a 16×16 matrix M which contains only 15 linearly independent variables of the density matrix since the sum of all populations is constant; i.e., $g_L + g_R + e_L + e_R = 1$. We therefore have to eliminate one variable and arrive at a 15×15 matrix A for which $|\dot{\rho}\rangle = A|\rho\rangle + |x_0\rangle$. Here the density matrix ρ is written as a vector $|\rho\rangle$ containing 15 elements. The steady-state situation where $|\dot{\rho}\rangle = 0$ is then given by $|\rho\rangle = -A^{-1}|x_0\rangle$. To arrive at the steady state absorption spectrum for each detuning δ of the laser with respect to the OTLS frequency ω_{eg}, we calculate $I(\delta) = \langle\rho_0|\rho\rangle = -\langle\rho_0|A^{-1}|x_0\rangle$ where $\langle\rho_0| = (0, e_L = 1, e_R = 1, 0, ..., 0)$. We therefore take the absorption (or fluorescence excitation) spectrum of the OTLS to be proportional to the spectrum of the total excited state population.

Apart from the steady state it would also be possible to look for the time-dependent evolution of an observable by diagonalizing the matrix A. This would allow us to calculate for example correlation functions. By introducing a second weak probe laser which is detuned with respect to the present pump laser, pump−probe spectra could be calculated[31] and more complex nonlinear phenomena such as the light shift[32] could be studied. This will be kept for future work.

3. Results and Discussion

We calculated steady-state absorption spectra of the coupled OTLS−VTLS system by inverting the Liouville matrix (Figure 2). For the sake of limiting the number of parameters, we will assume that the tunneling matrix element is equal in the ground and excited states of the OTLS, $\Delta_0 = \Delta_{0g} = \Delta_{0e}$. The results are generally presented as series of absorption spectra changing as a function of one control parameter, which can be the asymmetry, the tunneling matrix element, or the jump rate of the VTLS or the Rabi frequency of the OTLS. The laser frequency is plotted on the horizontal axis, the varying control parameter on the vertical axis, and the intensity of absorption is coded as a level of gray. This encoding is linear and saturates as black in several of the plots. For each plot, a few spectra are also given to give a feeling of the intensity-to-gray encoding. All spectra within each figure are plotted on the same scale.

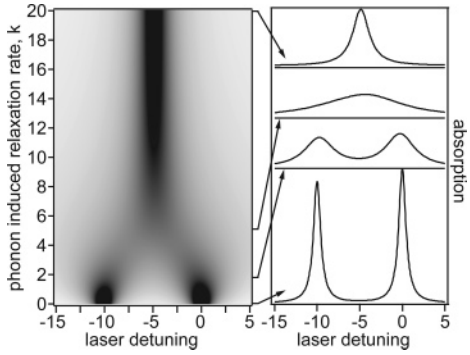

Figure 3. Sudden jump limit. The left part shows a two-dimensional representation of a stack of calculated absorption spectra. In this and the following figures, the gray scale gives the absorption intensity. The right panel shows absorption spectra, which are cross sections at the place of the arrows. The parameters of the present simulation in units of Γ are $\Omega = 0.1$, $\Delta_0 = 0$, $\Delta_e = 0$, $\Delta_g = 10$, and $T = 100$; the jump rate k is varied. Note the transition from a double peak at low jump rate (spectral diffusion) to a single line at high jump rate (motional narrowing). The two lines actually merge, as predicted by the semiclassical sudden-jump model of Kubo and Anderson.

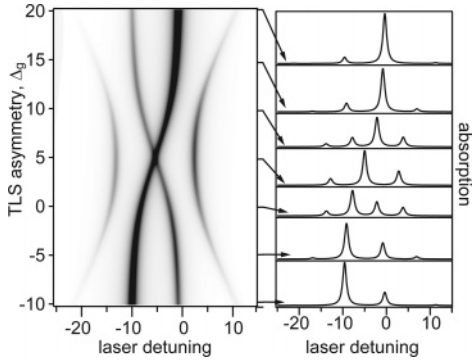

Figure 4. Weak tunneling. The parameters of the simulation in units of Γ are $\Omega = 0.1$, $\Delta_0 = 3$, $\Delta_e - \Delta_g = -10$, $k = 0.001$, and $T = 10$; the ground-state asymmetry is varied, and the difference in asymmetries remains fixed. One first notices the two main lines corresponding to gL $\rightarrow$ eL and gR $\rightarrow$ eR, which cross as the asymmetry of the VTLS changes sign. Note that the intensity of the lower tunnel state gD remains higher. In addition to those, the two-cross transitions gL $\rightarrow$ eR and gR $\rightarrow$ eL also appear as hyperbola-like arcs.

Hereafter, we discuss several limiting cases to illustrate the physics of the four-level system, first for low laser power and then for arbitrary excitation intensity. In all simulations, (angular) frequencies are given in units of Γ, the spontaneous emission rate.

In all the data presented here, absorption and excited populations were duly positive. We nonetheless observed some cases of negative absorption for extreme values of the parameters, in particular when the phonon-induced relaxation rate became too large. This points to some inconsistency in our set of assumptions. We particularly suspect the full neglect of real parts of the self-energies associated to the relaxation rates. Because calculating these shifts would require a specific model of phonon bath, we did not test this hypothesis and did not investigate the problem any further.

3.1. Sudden-Jump Limit. We first consider a VTLS without any coherent tunneling, with jump rate k from the right (upper) to the left (lower) well, split by $10 \times \Gamma$. Figure 3 shows the line shape in the high-temperature limit ($T = 100 \times \Gamma$) as a function of jump rate k. The profile changes from a two-line spectrum at low rate (slow modulation, spectral diffusion) to a single line at high rate (fast modulation, dephasing, and motional narrowing). Note that the two lines merge into a single one located at their center of gravity (actually, there is a second, broader component at the same frequency, whose weight quickly decreases as the jump rate increases). The width of the merged line decreases when the jump rate increases. This case has been well studied in the literature[35] and is well documented in magnetic resonance experiments.[26] Although uncommon in optical spectroscopy, it has been reported at least once for a single pentacene molecule in a *p*-terphenyl crystal.[33]

When the Rabi frequency is increased, all lines broaden because of optical saturation, but the picture remains qualitatively the same, in particular the rate at which the lines merge does not change.

3.2. Weak Tunneling. When a weak tunneling matrix element is introduced, two new transitions (gL $\rightarrow$ eR and gR $\rightarrow$ eL, see Figure 1) appear, in addition to the two first intense ones (gL $\rightarrow$ eL and gR $\rightarrow$ eR). Figure 4 presents optical line shapes for a tunneling matrix element $\Delta_0 = 3 \times \Gamma$, with a variation of the VTLS asymmetry in the ground state between -10 and $20 \times \Gamma$. Discussing the dependence of the spectra on VTLS asymmetry, we kept Bauer and Kador's experiments in mind (see next subsection). The VTLS asymmetry is varied by an applied electric field, because of a difference of dipole moment between the right and left wells of the VTLS. The difference between asymmetries of the VTLS in the excited and ground states of the OTLS, in contrast, arises only from the interaction between VTLS and OTLS and is independent of the applied electric field. We therefore took this difference $\Delta_e - \Delta_g$ to be constant and equal to $-10 \times \Gamma$. The Stark effect of the OTLS, arising from a difference in dipole moments of ground and excited states, was neglected. At the center of the plot, the VTLS asymmetries in ground and excited states are small and opposite. The two central lines are superimposed, and two additional lines split by $2(E_{eU} - E_{eD} + E_{gU} - E_{gD}) = 2(4\Delta_0^2 + \Delta_g^2)^{1/2} + 2(4\Delta_0^2 + \Delta_e^2)^{1/2}$ appear as hyperbolic arcs in Figure 4. This diagram is very similar to that presented in ref 10. We also note that the intensity of one of the two branches crossing in the center remains lower than that of the other one, with a ratio that depends on temperature. The lowest tunnel state is close to the right well for negative asymmetry but becomes close to the left well for positive asymmetry. In the center of the plot, it still has the highest population, because it has now become the gD tunneling state (see Figure 1), split by about $2\Delta_0$ from the gU state.

This picture changes dramatically when the Rabi frequency is increased. The additional arcs quickly lose relative intensity, which can be understood from their very weak saturation intensity. Indeed, at high excitation power, optical pumping takes place in the four-level system. The gL $\rightarrow$ eR transition populates the eR state, which quickly relaxes by spontaneous emission toward the gR state, where the system remains trapped because there is no resonant absorption from the latter state at the laser frequency. Only the weak VTLS relaxation rate k repopulates the initial gL state. The narrow central feature at the crossing of the two main traces becomes particularly intense at high Rabi frequency, as will be discussed later (section 3.5).

3.3. Bauer−Kador Case. A few years ago, Bauer and Kador[28,29] have observed a VTLS whose asymmetry could be varied with an applied electric field. Studying terrylene in *n*-hexadecane they actually measured intensity plots similar to those of Figure 4. We have fitted their data with our model, and the results are presented in Figure 5. The best agreement is obtained with a difference of asymmetries of $7.5 \times \Gamma$, a tunneling matrix element of $94 \times \Gamma$, a jump rate of about $0.01 \times \Gamma$, and a laser intensity of about $0.1 \times \Gamma$. The latter two

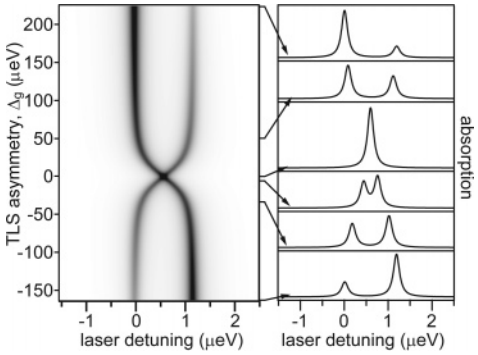

Figure 5. Bauer−Kador case. The parameters of the simulation in units of Γ are Ω = 0.1, Δ_0 = 94, $\Delta_e - \Delta_g$ = 7.5, k = 0.01, and T = 1031, whereas in real units they amount to Γ = 40 MHz = 0.16 μeV,[34] Δ_0 = 15 μeV, $\Delta_e - \Delta_g$ = 300 MHz = 1.2 μeV, and T = 1.9 K = 165 μeV. The ground-state asymmetry is varied, and the difference in asymmetries remains fixed. The parameters have been determined by fitting the splitting of the lines and the intensities reported in refs 28 and 29. The two main lines behave as in Figure 4, and the cross transitions are very weak and remote because the tunneling element is very large.

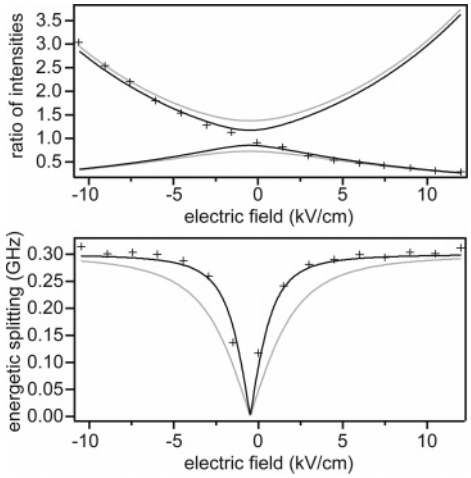

Figure 6. Ratio of intensities and spectral splitting of the two components for a single molecule discussed in refs 28 and 29. The crosses represent experimental data points, the gray lines the calculated values based on the parameters of refs 28 and 29, and the black lines the calculated values based on the parameters given in Figure 5.

parameters can be varied over a certain range without changing the quality of the fit. The temperature was given in the paper as 165 × Γ. The tunneling matrix element Δ_0 was found to be about 100 × Γ, 0.2 cm^{-1}. Although rather large, such values are not uncommon in the broad distribution of VTLSs in glasses.[35] The plot of Figure 5 only shows the two central lines. The hyperbolic arcs, although present, are well outside the scale of the presented plot and much weaker than the central structures. They would have been difficult to detect on the experimental spectra at low laser power.

Figure 6 compares the splitting and ratio of intensities of the two central lines measured experimentally[28,29] (crosses) and the results of a simple analytical calculation with our parameters (black lines). The resulting parameters from our fits are significantly different from those found by Bauer and Kador,[28,29] which would lead to the gray lines in Figure 6. The ratio of intensities results from the ratio of the ground-state populations in the up and down states, $g_D/g_U = \exp((E_{gU} - E_{gD})/k_BT)$ for the upper line and g_U/g_D for the lower line. The energetic splitting is simply the difference in energy of the two transitions

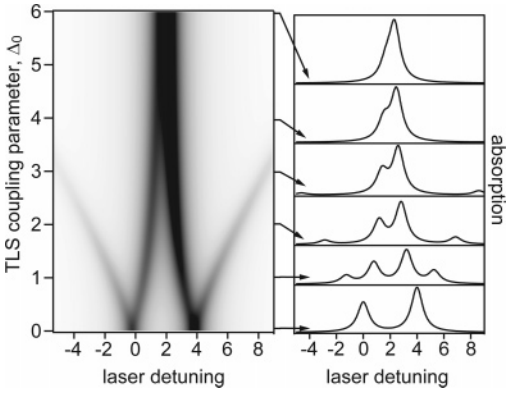

Figure 7. Variable tunneling element. The parameters of the simulation in units of Γ are Ω = 0.01, Δ_e = 0, Δ_g = −4, k = 0.01, and T = 10. The tunneling matrix element Δ_0 is varied. The spectrum changes from two lines at zero tunneling element (sudden jump model) to four lines. The two central lines overlap for large Δ_0 but do not really merge, at least for low Rabi frequency. The two cross transitions (corresponding to the arcs of Figure 4) quickly drift apart and lose oscillator strength for strong tunneling.

$(E_{eU} - E_{gU}) - (E_{eD} - E_{gD}) = (4\Delta_0^2 + \Delta_e^2)^{1/2} - (4\Delta_0^2 + \Delta_g^2)^{1/2}$ and k_B is the Boltzmann constant.

The agreement between experiment and analytical result is very good. Note that the intensity ratio of the two lines follows two different curves (upper part of Figure 6), one being the inverse of the other. The remarkable features of these data are not only the possibility to tune the asymmetry with an applied field but also the very large value of Δ_0, about 100 times the line width. The cross transitions (not visible in Figure 5) would have been too weak to appear in the experimental conditions but could have been found at high laser power. They would have provided a more accurate determination of the tunneling element Δ_0.

3.4. Variable Tunneling Element. We can also study the line shape as a function of the tunneling matrix element Δ_0. Figure 7 shows an intensity plot for a constant asymmetry of −4 × Γ in the ground state, 0 in the excited state. The tunneling element varies between 0 and 6 × Γ, the jump rate between tunnel states is 0.01 × Γ, and the temperature is 10 × Γ. For zero tunneling, the system switches between left and right wells, giving rise to two lines split by 4 × Γ. When the tunnel element is increased, each one of these lines splits in two components (left-to-left splits into left-to-down and left-to-up, see Figure 1). For very large Δ_0, two of the new lines gain intensity and overlap in the center; they correspond to down-to-down and up-to-up transitions, which differ only by a slight shift due to the asymmetry in the ground OTLS state. The two other transitions drift apart and lose oscillator strength.

Again, this picture is very sensitive to Rabi frequency. Because of optical pumping, the relative intensity of the lateral lines decreases quickly with increasing laser power and their widths increase because of saturation.

3.5. Variable Rabi Frequency. Figure 8 shows the variation of the line shape with a given asymmetry of 10 × Γ in the ground state, 0 in the excited state, and a tunneling matrix element of 2 × Γ. The jump rate k is 0.01 × Γ and the temperature 100 × Γ. The Rabi frequency is varied from 0 to 10 × Γ. The plot starts from a four-line spectrum at low laser power, corresponding to the four possible transitions. The two middle lines, corresponding to gD → eD and gU → eU transitions (see Figure 1) merge when intensity is increased, instead of superimposing. Their frequency drift is quite apparent on the plot, where the two lines resemble a swallow's tail. The

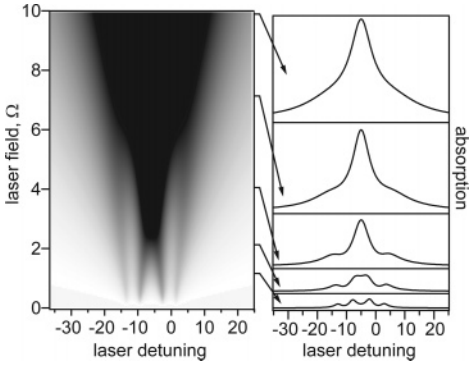

Figure 8. Variable Rabi frequency. The parameters of the simulation in units of Γ are $\Delta_0 = 2$, $\Delta_e = 0$, $\Delta_g = 10$, $k = 0.01$, and $T = 100$; Ω is varied. Note that the two central lines now merge when the Rabi frequency increases, which indicates that the laser creates a new coherent superposition of tunneling states.

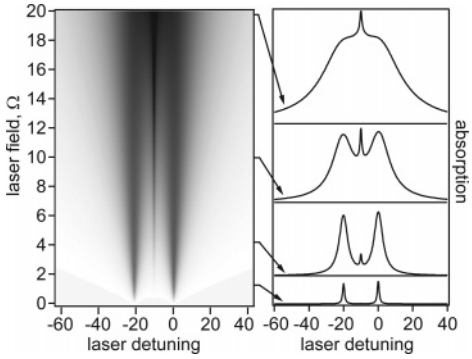

Figure 9. Variable Rabi frequency. The parameters of the simulation in units of Γ are $\Delta_0 = 0.3$, $\Delta_e = -10$, $\Delta_g = 10$, $k = 0.01$, and $T = 100$; Ω is varied. Now, the two cross transitions have been chosen degenerate, weak (Δ_0 is weak), and coincide with the center of the spectrum. They do not appear at weak laser power but quickly grow as a single line proportional to the square of the Rabi frequency, which indicates a two-photon nonlinear process. The corresponding line remains narrow and saturates only at very high Rabi frequency.

merging of these lines can be interpreted as the creation of a new coherent superposition of tunnel states by laser pumping. The resulting central line at high Rabi frequency corresponds to the central feature mentioned in section 3.2 and discussed below. On the other hand, the external lines corresponding to gD → eU and gU → eD transitions start to shift apart at low laser power, before being broadened by saturation and absorbed by the main line.

Figure 9 presents a special case where the two middle transitions previously discussed are accidentally degenerate. The parameters are an asymmetry of $10 \times \Gamma$ in the ground state, $-10 \times \Gamma$ in the excited state, a tunneling matrix element of $0.3 \times \Gamma$, a jump rate k of $0.01 \times \Gamma$, and a temperature of $100 \times \Gamma$. For such a weak value of the tunnel element, the degenerate middle lines are almost forbidden and are too weak at low laser power to appear on the plot. However, as the power is increased, they appear and eventually dominate the whole spectrum, by remaining very sharp, even at high laser power. Their saturation intensity is much larger than that of the allowed external lines. The intensity of this middle line can be seen as a two-photon absorption, where in a first step one laser photon is absorbed in a gD → eD transition. This transition is almost a left to right transition and is therefore weak. The second step consists of spontaneously emitting one photon in an eD → gU transition which is strongly allowed as it is almost a right to right transition. Finally, a second, degenerate laser photon is absorbed in a gU → eU transition, ending up with net laser absorption. This last transition is again a weak, almost right to left transition. If we increase the phonon jump rate, we observe a decrease of the intensity of the sharp middle line relative to the two broad external lines. This decrease results from an impaired absorption of a second photon as the gU state is depleted by the phonons and part of its population is transferred to the gD state. This two-photon spectral feature, reminiscent of the one found and explained by Hettich et al.,[21] could be used to determine the relaxation rate between VTLS states once the tunneling matrix element is known, or vice versa.

4. Conclusion and Outlook

We have proposed a general mathematical treatment of a four-level system representing a single OTLS coupled to a single VTLS in an arbitrary laser field, representing, for example, a single fluorescent molecule in a disordered matrix. Despite its apparent simplicity, the coupled four-level system presents a surprising richness and complexity. Among the several phenomena encountered, we found motional narrowing, cross transitions between different levels of the VTLS, induced by changes of the tunneling potential between the ground and excited OTLS-states, optical pumping and saturation, and nonlinear effects at high laser fields.

As we have shown, these complex effects give rise to characteristic features in the absorption spectra of single molecules, which compare well with earlier experimental data. However, more subtle signatures, such as autocorrelations, cross correlations or anticorrelations of fluorescence photons could be sought, in studies similar to that presented by Hettich et al.[21] To model these higher-order functions, one should solve the time-dependent evolution of the density matrix by diagonalizing matrix M (see Figure 2) and expressing the excited-state population as a function of time after measurement of a fluorescence photon, with possible spectral selection. These more complex calculations will be the subject of future work.

Acknowledgment. The present subject arose from a discussion with Prof. R. J. Silbey in May 2005, upon one of his visits to Leiden. We dedicate this article to him as a token of deep reverence and appreciation. This work was supported by the European IST-project CHIC (Number 2001-33578) and is part of the research program of the Stichting voor Fundamenteel Onderzoek der Materie, which is part of the NWO.

References and Notes

(1) Feynman, R. P.; Vernon, F. L.; Hellwarth, R. W. *J. Appl. Phys.* **1957**, *28* (1), 49−52.
(2) Wu, F. Y.; Ezekiel, S.; Ducloy, M.; Mollow, B. R. *Phys. Rev. Lett.* **1977**, *38* (19), 1077−1080.
(3) Lounis, B.; Jelezko, F.; Orrit, M. *Phys. Rev. Lett.* **1997**, *78* (19), 3673−3676.
(4) Kubo, R. *J. Phys. Soc. Jpn.* **1954**, *9* (6), 935−944.
(5) Anderson, P. W. *J. Phys. Soc. Jpn.* **1954**, *9* (3), 316−339.
(6) Silbey, R.; Kassner, K. *J. Lumin.* **1987**, *36* (4−5), 283−292.
(7) de Vries, H.; Wiersma, D. A. *J. Chem. Phys.* **1980**, *72* (3), 1851−1863.
(8) Geva, E.; Skinner, J. L. *J. Phys. Chem. B* **1997**, *101* (44), 8920−8932.
(9) Reineker, P.; Morawitz, H.; Kassner, K. *Phys. Rev. B* **1984**, *29* (8), 4546−4561.
(10) Reineker, P.; Kassner, K. Model Calculation of Optical Dephasing in Glasses. In *Optical Spectroscopy of Glasses*; D. Reidel Publishing Co.: Dordrecht, 1986; pp 65−147.
(11) Mori, H. *Prog. Theor. Phys.* **1965**, *33* (3), 423.
(12) Redfield, D. *Phys. Rev. Lett.* **1971**, *27* (11), 730.
(13) de Bree, P. D.; Wiersma, D. A. *J. Chem. Phys.* **1979**, *70* (2), 790−801.
(14) Cohen-Tannoudji, C.; Dupont-Roc, J.; Grynberg, G. *Atom-Photon Interactions;* Wiley: New York, 1992.

(15) Mukamel, S. *The Principles of Nonlinear Optical Spectroscopy;* Oxford University Press: Oxford, 1995.
(16) Plakhotnik, T. *J. Chem. Phys.* **2001**, *114* (13), 5631−5636.
(17) Phillips, W. A. *J. Low Temp. Phys.* **1972**, *7* (3−4), 351−360.
(18) Anderson, P.; Halperin, B.; Varma, C. *Philos. Mag.* **1972**, *25*, 1−9.
(19) Phillips, W. *Amorphous solids, Low-Temperature Properties;* Springer-Verlag: Berlin, 1981.
(20) Boiron, A.-M.; Tamarat, P.; Lounis, B.; Brown, R.; Orrit, M. *Chem. Phys.* **1999**, *247*, 119−132.
(21) Hettich, C.; Schmitt, C.; Zitzmann, J.; Kühn, S.; Gerhardt, I.; Sandoghdar, V. *Science* **2002**, *298*, 385−389.
(22) Hofmann, C.; Ketelaars, M.; Matsushita, M.; Michel, H.; Aartsma, T.; Köhler, J. *Phys. Rev. Lett.* **2003**, *90* (2), 013004.
(23) Sild, O., Haller, K., Eds. *Zero-Phonon Lines;* Springer-Verlag: Berlin, 1988.
(24) Golding, B.; Graebner, J. Relaxation Times of Tunneling Systems in Glasses. In *Amorphous solids, Low-Temperature Properties*; Springer-Verlag: Berlin, 1981; pp 107−134.
(25) Shen, Y. *The Principles of Nonlinear Optics;* Wiley: New York, 1984.
(26) Abragam, A. *The Principles of Nuclear Magnetism;* Oxford University Press: Oxford, 1961.
(27) Hofmann, C.; Nicolet, A.; Kol′chenko, M. A.; Orrit, M. *Chem. Phys.* **2005**, *318* (1−2), 1−6.
(28) Bauer, M.; Kador, L. *J. Chem. Phys.* **2003**, *118* (20), 9069−9072.
(29) Bauer, M.; Kador, L. *J. Lumin.* **2004**, *107* (1−4), 32−37.
(30) Skinner, J. L.; Trommsdorff, H. P. *J. Chem. Phys.* **1988**, *89* (3), 897−907.
(31) Jelezko, F.; Lounis, B.; Orrit, M. *J. Chem. Phys.* **1997**, *107* (6), 1692−1702.
(32) Tamarat, P.; Jelezko, F.; Brunel, C.; Maali, A.; Lounis, B.; Orrit, M. *Chem. Phys.* **1999**, *245* (1−3), 121−132.
(33) Talon, H.; Fleury, L.; Bernard, J.; Orrit, M. *J. Opt. Soc. Am. B* **1992**, *9* (5), 825−828.
(34) Moerner, W.; Plakhotnik, T.; Irngartinger, T.; Croci, M.; Palm, V.; Wild, U. *J. Phys. Chem.* **1994**, *98*, 7382−7389.
(35) Bordat, P.; Orrit, M.; Brown, R.; Würger, A. *Chem. Phys.* **2000**, *258*, 63−72.